Line Tension at Fluid Membrane Domain Boundaries Measured by Micropipette Aspiration

Aiwei Tian, Corinne Johnson, Wendy Wang, and Tobias Baumgart*

Department of Chemistry, University of Pennsylvania, Philadelphia, Pennsylvania 19104, USA

(Received 23 December 2006; published 16 May 2007)

Line tension is a determinant of fluid phase domain formation kinetics and morphology in lipid bilayer membranes, which are models for biological membrane heterogeneity. We describe the first direct measurement of this line tension by micropipette aspiration. Our data are analyzed with a model that does not rely on independently measured (and composition dependent) secondary parameters, such as bending stiffness or membrane viscosities. Line tension is strongly composition dependent and decreases towards a critical consolute point in a quasiternary room temperature phase diagram.

DOI: 10.1103/PhysRevLett.98.208102 PACS numbers: 87.16.Dg, 46.70.Hg, 87.14.Cc, 87.64.Tt

It has been suggested that biomembrane domains, often termed rafts, play important roles in cellular membrane function [1,2]. Biological membrane fluid phase coexistence can be experimentally modeled via liquid disordered (L_d) and liquid ordered (L_o) phases in membranes self-assembled from synthetic or natural purified lipids. Line tension at the domain phase boundary controls the kinetics of phase separation and domain sizes. *In vivo*, line tension could be an essential control parameter for regulation of lateral compartmentalized membrane-localized signaling complexes.

Lipid bilayer line tensions can be divided into those that are measured at a bilayer membrane edge (membrane pore) and those that are found at the domain boundary of phase separated but otherwise continuous membranes. These *edge tensions* were determined both experimentally [3–5] and theoretically [6], with values near $\sim$10 pN. Recently, shape analysis of giant unilamellar vesicles yielded rough line tension estimates for fluid-fluid phase coexistence in the range of $\sim$1 pN [7,8]. Approximate line tension values were obtained by determining dimensionless fit parameters through comparison of model membrane shapes and computed shapes using theory developed by Juelicher and Lipowsky [9]. Rescaling of these fit parameters with vesicle dimension and literature value estimates of bending stiffness allowed determining lateral tensions, bending stiffness differences, and line tension in vesicles with fluid phase coexistence [7,8]. The problem with generalizing this approach is that bending stiffness and other mechanical properties depend on the composition of coexisting phases, which are thus far only known for selected average compositions [10,11]. Also, to our knowledge, no attempts have yet been made to measure absolute values of bending stiffness in domains of phase separated lipid membranes. In principle, domain shape relaxation of equilibrium or nonequilibrium shape fluctuations can be used to measure fluid domain boundary line tension [12]. However, membrane domain viscosities, which are strongly composition dependent (see, e.g., [13]) and would have to be measured independently, influence relaxation kinetics [12].

We used giant unilamellar vesicles prepared by electroswelling, as described [14], consisting of lipid mixtures containing components such as di-oleoyl-PC (DOPC), diphytanoyl-PC (DPhyPC), di-palmitoyl-PC (DPPC), egg sphingomyeline (ESM), cholesterol (Chol), and the ganglioside GM1, which were obtained from Avanti Polar Lipids, Inc. (Alabaster, AL) and used without purification. Micropipettes for vesicle aspiration were obtained from glass capillaries with a micropipette puller, clipped by means of a microforge, and conditioned with fatty-acid free bovine serum albumin (BSA, Sigma, St. Louis, MO) to avoid membrane adhesion. The fluorophores Texas Red-DPPE (TR-PE) and fluorescence labeled (Alexa-488) cholera toxin subunit B (CTB) were from Invitrogen (Carlsbad, CA). Lipid mixtures contained 1 mol% GM1 and 0.5 mol% TR-PE to allow fluorescence observation of vesicles prepared in 100 mM sucrose solution [additionally containing 2 mM dithiothreitol (DTT) to reduce photochemical effects [15] and 0.02% sodium azide]. CTB-GM1 binding allowed us to image the L_o phase [16], whereas the L_d phase could be visualized through the L_d phase targeting property of TR-PE. Since it was previously found that CTB binding to GM1-containing vesicles can slightly shift phase boundaries [7], the phase behavior of quasiternary mixtures was determined in the presence of GM1 and CTB.

For micropipette aspiration, 100 μl giant unilamellar vesicle (GUV) dispersion was diluted (typically 1:10 with the GUV swelling solution specified above, to decrease GUV concentration) and injected into a pipette aspiration chamber. Bulk flow was sufficiently suppressed to exclude artifactual contributions of Stokes friction to the force equilibrium of aspirated vesicles. Because of the relatively low aspiration pressures used in our experiments, particular care was exerted regarding zero pressure calibration, which we performed by the standard method of observing small (fluorescent) particles move in the pipette. The zero pressure was recalibrated after every vesicle aspiration and after every spatial translation of the pipette. Vesicles were imaged by fluorescence confocal microscopy (Olympus, FV300) and image analysis was performed using Matlab (Mathworks, Natick, MA). All

experiments were performed at room temperature (22 ± 1 °C).

After identifying dumbbell shaped giant vesicles (i.e., vesicles deflated from spherical shape) in the vesicle dispersion, GUVs were micropipette aspirated (see Fig. 1) to initially yield a spherical vesicle shape outside the pipette and a tongue (projection) within the pipette. Aspiration via the L_d phase was avoided in routine measurements since it often led to fragmentation during elongation of the cylindrical aspirated projection. Fragmentation, i.e., budding transitions of the projection, had to be avoided due to potential pressure drops in the micropipette interior caused by congesting budded daughter vesicles that were observed to slowly move away from the mother vesicle into the pipette.

Aspiration of GUVs into the pipette interior was observed to be a two-step, pressure dependent process. Typically, at low pressures, vesicles were observed to attach to the pipette mouth showing membrane curvature in the membrane patch covering the mouth not significantly different from the nonaspirated vesicle [i.e., almost zero projection lengths were found, see Fig. 1(e)]. Upon increasing the suction pressure (by lowering the water reservoir connected to the pipette), a sudden (within less than 1 s) transition from approximately zero projection length to a maximal length was observed at the critical aspiration pressure and the aspirated dumbbell became spherical during this transition. For the vesicle depicted in the sequence Fig. 1(b)–1(e), this critical aspiration pressure was 16.1 ± 0.2 Pa. This instability is similar to earlier micropipette aspiration of membranes without line tension contribution, as in red cells [17]. The suction pressures where these instabilities were observed were larger when aspirating the L_o phase, compared to the L_d phase. For example, for vesicles with composition #3 (see below) the ratio of critical aspiration pressures of L_o and L_d phase (measured with the same pipette in domains of the same vesicle) was 2.5 ± 0.23 (for 10 vesicles). This observation is likely due to higher bending stiffness of L_o versus L_d phase [7,8].

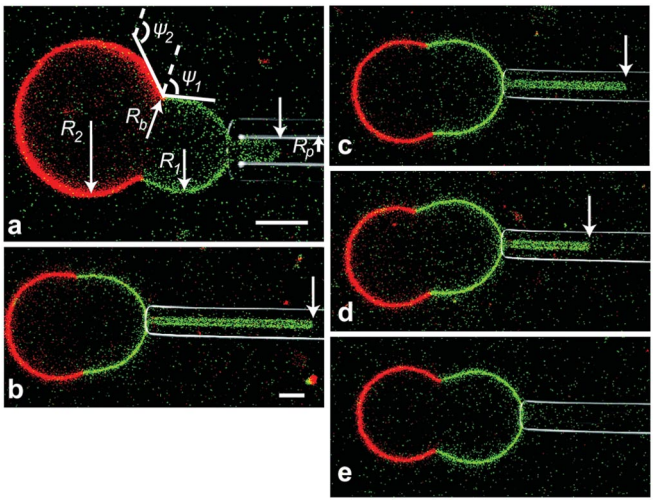

FIG. 1 (color). (a) Demonstration of a typical line tension measurement. One domain (typically the L_o domain, as depicted in green) of a dumbbell shaped vesicle was aspirated with a micropipette. The L_o domain was labeled with CTB-Alexa 488 and the L_d domain was labeled by Texas Red-DPPE (TR-PE). R_p and R_b are the radii of the pipette and the phase boundary; R_1 and R_2 are curvature radii of partially aspirated and nonaspirated domain; ψ_1 and ψ_2 are the tangent angles immediately before and after the phase boundary; the tip of the aspirated vesicle projection is marked with a vertical arrow. (b)–(e) Time-lapse series of an experiment where one vesicle was aspirated using four different aspiration pressures: (b) 2.7 Pa, (c) 1.9 Pa, (d) 1.0 Pa, and (e) 0.9 Pa (all values ±0.2 Pa). For these aspiration pressures, the line tension obtained from vesicle geometry, pipette diameter, and aspiration pressure was roughly the same: (b) 3.1 ± 0.2 pN, (c) 3.0 ± 0.3 pN, (d) 3.0 ± 0.6 pN. (e) Vesicle beyond critical releasing instability. Scale bar: 5 μm.

After initial aspiration, projection lengths were typically decreased to yield dumbbell shaped vesicles similar to the GUVs shown in Fig. 1. Projection lengths were observed to be reversibly dependent on the applied suction pressure. Vesicles depicted in Fig. 1 all refer to mechanical equilibrium. The projection lengths decreased after decreasing suction pressure until a new mechanical equilibrium was reached.

Projection lengths could not be decreased beyond a critical value dependent on area fraction and reduced volume of the aspirated vesicle. Below this value, mechanical stability of a cylindrical aspirated vesicle membrane typically could not be reached and the projection would retract from the pipette interior, with the vesicle remaining attached to the pipette mouth at equilibrium [see Fig. 1(e)]. The critical releasing pressures associated with these instabilities were significantly smaller than those needed for initial formation of a cylindrical aspirated vesicle domain: compare the critical aspiration pressure of 16.1 ± 0.2 Pa and critical releasing pressure of 0.9 ± 0.2 Pa for the vesicle depicted in Fig. 1(b)–1(e). Both Figs. 1(a) and 1(d) show projection lengths immediately before the critical releasing instability is reached.

We developed an analysis scheme based on the measurement of the two meridianal tangent angles ψ_1 and ψ_2 of L_o and L_d phase at the phase boundary, boundary and pipette radius R_b and R_p, respectively, and suction pressure $\Delta P = P_o - P_p$, where P_o is the pressure outside vesicle and pipette, and P_p is the pressure inside the pipette [see Fig. 1(a)]. Additional geometric vesicle parameters are the radii R_i of near-spherical domains $i = 1, 2$, outside the pipette. In the following, we assume dumbbell vesicle mechanical equilibria to primarily depend on the following mechanical parameters: lateral tensions Σ_i, suction pressure ΔP, vesicle normal pressure difference outside the pipette $\Delta P_v = P_i - P_o$ (where P_i is the inner vesicle pressure), and line tension σ, whereas bending stiffness contributions were neglected. This approximation is based on the zero order solution of a recent boundary layer

analysis [18], which is accurate if phase boundary energies are significantly larger compared to the bending energy. Assuming that the lateral membrane tension Σ_1 within the domain that is aspirated is equal inside and outside the pipette [19], the suction pressure is related to ΔP_v through $\Delta P/\Delta P_v = R_1/R_p$, where R_1 is the radius of the domain adjacent to the pipette mouth [see Fig. 1(a)]. A force balance within the plane containing the domain boundary yields $\sigma/R_b = \Sigma_1 \cos\psi_1 - \Sigma_2 \cos\psi_2$, from which we obtain with $2\Sigma_i = \Delta P_v R_i$ (for each domain i) a relationship between line tension and ΔP_v, $\sigma = 0.5\Delta P_v R_b^2(\cot\psi_1 - \cot\psi_2)$ [7,8]. Replacing ΔP_v by ΔP and eliminating R_1 yields the following linear relation between ΔP and σ:

$$\sigma = \Delta P \frac{R_b^2 R_p \sin\psi_1}{2(R_b - R_p \sin\psi_1)}(\cot\psi_1 - \cot\psi_2). \qquad (1)$$

Equation (1) was used to relate the adjusted suction pressure and the resulting vesicle geometry to the line tension in a particular vesicle. Before we examined the composition dependence of line tension for mixtures referring to a quasiternary phase diagram with fluid phase coexistence, we first tested the reliability of this method with different vesicle geometries, obtained from varying aspiration pressures. A vesicle was aspirated at a range of suction pressures from 1 to 2.7 ± 0.2 Pa, as shown in Fig. 1(b)–1(d). Identical line tension values were obtained from the same vesicle in different geometries, within the errors of our approximations and measurement. We then proceeded to demonstrate quantitatively the composition dependence of phase boundary line tension. We examined the line tensions of GUVs made of DOPC:Chol:ESM mixtures with five compositions within the L_o-L_d phase coexistence region as Fig. 2 shows. In this partial phase diagram, we determined the upper (referring to high cholesterol content) boundary of the binary miscibility gap [20] and the area fractions of ordered and disordered phases, from which the location of a critical mixing or demixing (consolute) point could be estimated. Five compositions were chosen, one near the critical point and the remaining ones along a line roughly orthogonal to the expected tie line directions (see Fig. 2). This compositional trajectory roughly crosses the middle of the expected tie lines [20], since the majority of vesicles showed similar areas of L_o and L_d phase for all five compositions (data not shown). Typically, a significant (roughly 10%) spread of area fractions was found in each vesicle preparation, indicating compositional differences among individual vesicles. This difference in composition is also reflected in the spread of line tension value histograms for every measured composition, as shown in Fig. 3.

For each composition, 20 vesicles were examined. Histograms demonstrating the large spread of individual measurements summarize our results in Fig. 3(a)–3(e). Average values of line tension are shown in Fig. 3(f). These average values decreased from 3.3 pN (farthest away from the critical point) to 0.5 pN (closest to the critical point), see Fig. 3(f). Average line tension values therefore change over almost 1 order of magnitude, de-

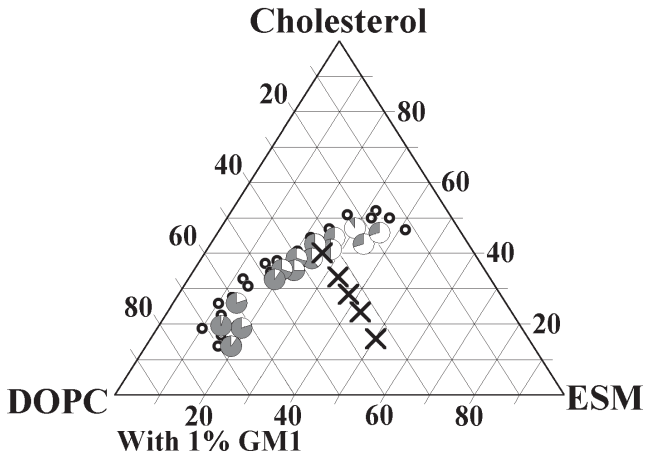

FIG. 2. Partial room temperature phase diagram of the DOPC:Chol:ESM mixture. The circles demonstrate the upper boundary of the liquid coexistence region. Open circles indicate homogeneous vesicles; pie diagrams indicate phase separated vesicles, in which gray color quantifies the average area fraction of the disordered phase. From the area fractions and the phase boundary the approximate location of an upper critical consolute point can be identified. Five compositions were chosen including this area as well as four more compositions lying on a trajectory orthogonal to the expected tie line directions. The ratios of DOPC:Chol:ESM for each composition from the top to bottom are (1): 0.34:0.4:0.26; (2): 0.34:0.33:0.33; (3): 0.34:0.28:0.38; (4): 0.34:0.23:0.43; (5): 0.34:0.16:0.5, respectively, as indicated by crosses.

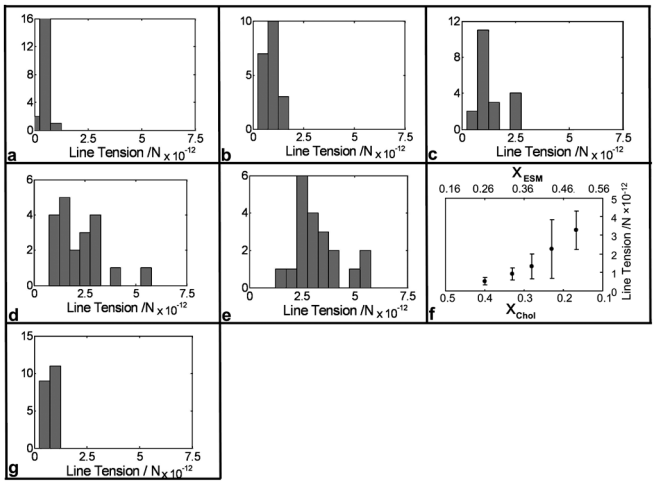

FIG. 3. (a)–(e) Histograms of line tension values for the five compositions (1)–(5). 20 vesicles were measured for each composition. (f) The average value of line tensions are plotted vs the mole ratio of cholesterol and ESM. From left to right are the compositions (1)–(5), and the corresponding average line tension values are 0.5, 0.9, 1.3, 2.3, 3.3 pN, respectively. (g) Histogram of line tensions of 20 vesicles with composition DPhyPC : Chol : DPPC = 3:2.75:4.25. The average value is 0.7 pN.

pending on the vesicle composition, and decrease continuously towards the mixing-demixing critical point.

Recently, a closed loop fluid-fluid miscibility gap has been described in a similar ternary lipid mixture [11]. In case of a closed loop miscibility gap, in addition to a high cholesterol critical point, an additional critical point is expected near our lowest cholesterol composition [20]. In that case, line tension along the compositional trajectory chosen for our measurements should assume a maximum in the middle of the miscibility gap and decrease towards both critical points. Clearly, this behavior is not reflected by our measurements [Fig. 3(f)]. However, the data of Ref. [11] show that a closed loop miscibility gap exists *above* the chain melting temperature T_m of the long chain saturated, ordered phase preferring lipid, whereas *below* T_m, a three phase triangle, where L_o, L_d, and a gel phase coexist, neighbors the L_o-L_d phase binary miscibility gap. The phase diagram obtained in Ref. [11] indicates that the terminal tie line of the binary L_o-L_d coexistence region adjacent to the three phase triangle refers to a significant compositional difference between L_o and L_d phase. The line tension associated with a phase boundary in vesicles with composition referring to this terminal tie line therefore can be large. The large line tension obtained from our measurements in vesicles with lowest cholesterol composition therefore suggests that at room temperature, a three phase triangle borders the L_o-L_d coexistence region in the DOPC:Chol:ESM phase diagram. Since our measurements were performed at room temperature, significantly below T_m of ESM, this interpretation is in accordance with Ref. [11]. Three phase coexistence regions are typically difficult to identify by fluorescence microscopy imaging alone [21].

Next we examined to what extent line tensions depend on the lipid species used for ternary and quasiternary lipid mixtures. To that end, we measured line tension within the DPhyPC:Chol:DPPC mixture, see Fig. 3(g), for a composition roughly referring to the middle of the L_o-L_d miscibility gap at room temperature [11]. The line tension of the composition referring to the middle of the miscibility gap in the DOPC:Chol:ESM mixture (1.3 pN) is significantly larger than line tensions measured for vesicles consisting of DPhyPC:Chol:DPPC (0.7 pN). Membrane phase boundary line tensions are due in part to a thickness mismatch of L_o and L_d phase [22]. It might be possible to relate the composition and species dependence of line tension to this thickness difference by means of atomic force microscopy measurements of the membrane height profile across the phase boundary.

Our method to measure line tensions is suitable for magnitudes of this parameter that will deform vesicles into dumbbells with domain shapes that approximate truncated spheres. This situation is found when bending energy is small compared to phase boundary line energy, i.e., $\kappa \ll \sigma R_0$, where κ is the bending stiffness and R_o is the vesicle radius. Accordingly, our method is expected to be accurate for line tensions larger than on the order of 0.1 pN. We have shown that line tensions in quasiternary lipid mixtures are composition dependent and decrease towards a critical mixing-demixing point of the L_o-L_d miscibility gap. We expect that our approach can contribute to the identification of membrane minority components that influence line tension, i.e., line active components. Such molecules could be important as regulators of lateral heterogeneity in biological membranes.

This work was supported in part by the NSF sponsored UPenn Materials Research Science and Engineering Center (MRSEC), Grant No. DMR05-20020.

*Author to whom correspondence should be addressed.
Current address: Department of Chemistry, University of Pennsylvania, Philadelphia, PA, USA.
Email address: baumgart@sas.upenn.edu

[1] K. Simons and E. Ikonen, Nature (London) **387**, 569 (1997).
[2] M. Edidin, Annu. Rev. Biophys. Biomol. Struct. **32**, 257 (2003).
[3] P. H. Puech *et al.*, Phys. Rev. Lett. **90**, 128304 (2003).
[4] D. V. Zhelev and D. Needham, Biochim. Biophys. Acta **1147**, 89 (1993).
[5] E. Karatekin *et al.*, Biophys. J. **84**, 1734 (2003).
[6] J. de Joannis, F. Y. Jiang, and J. T. Kindt, Langmuir **22**, 998 (2006).
[7] T. Baumgart, S. T. Hess, and W. W. Webb, Nature (London) **425**, 821 (2003).
[8] T. Baumgart *et al.*, Biophys. J. **89**, 1067 (2005).
[9] F. Juelicher and R. Lipowsky, Phys. Rev. E **53**, 2670 (1996).
[10] S. L. Veatch *et al.*, Biophys. J. **86**, 2910 (2004).
[11] S. L. Veatch, K. Gawrisch, and S. L. Keller, Biophys. J. **90**, 4428 (2006).
[12] D. J. Benvegnu and H. M. McConnell, J. Phys. Chem. **96**, 6820 (1992).
[13] N. Kahya *et al.*, J. Biol. Chem. **278**, 28 109 (2003).
[14] L. Mathivet, S. Cribier, and P. F. Devaux, Biophys. J. **70**, 1112 (1996).
[15] A. G. Ayuyan and F. S. Cohen, Biophys. J. **91**, 2172 (2006).
[16] A. T. Hammond *et al.*, Proc. Natl. Acad. Sci. U.S.A. **102**, 6320 (2005).
[17] R. P. Rand and A. C. Burton, Biophys. J. **4**, 115 (1964).
[18] J. M. Allain and M. Ben Amar, Eur. Phys. J. E **20**, 409 (2006).
[19] R. Kwok and E. Evans, Biophys. J. **35**, 637 (1981).
[20] S. L. Veatch and S. L. Keller, Biochim. Biophys. Acta **1746**, 172 (2005).
[21] S. L. Veatch and S. L. Keller, Phys. Rev. Lett. **94**, 148101 (2005).
[22] S. A. Akimov *et al.*, J. Electroanal. Chem. **564**, 13 (2004).